Title:

Cholinergic suppression of sharp wave-ripples impairs hippocampus-dependent spatial memory

Author(s): Przemyslaw Jarzebowski[1], Clara S. Tang[1], Ole Paulsen, Y. Audrey Hay

Author affiliation: Department of Physiology, Development and Neuroscience, Physiological Laboratory, Cambridge, CB2 3EG, UK.

[1] Contributed equally

Abbreviated title: Cholinergic modulation of hippocampal memory

Corresponding author email address: ah831@cam.ac.uk, op210@cam.ac.uk

Number of pages: 44

Number of figures: 5 + 3

Number of tables: 0

Number of multimedia: 0

Number of 3D models: 0

Number of words for Abstract: 149

Introduction: 829

Discussion: 1732

Conflict of interest statement

The authors declare no conflicts of interest.

Acknowledgements: We thank Drs Julija Krupic and Mohamady El Gaby for introducing us to recordings in freely moving animals.

Author contributions: All authors designed research; C.S.T., P.J. and Y.A.H. performed research; C.S.T., P.J. and Y.A.H. analyzed data; all authors wrote the paper.

Funding: This work was supported by the Biotechnology and Biological Sciences Research Council [grant numbers BB/N019008/1 and BB/P019560/1]. C.S.T. was supported by a Cambridge Trust Scholarship. P.J. is supported by a Biotechnology and Biological Sciences Research Council Doctoral Training Programme studentship.

Abstract

The hippocampus plays a central role in long-term memory formation, and different hippocampal network states are thought to play distinct roles in this process. These network states are controlled by neuromodulatory inputs, in particular the cholinergic input from the medial septum. Here, we used optogenetic stimulation of septal cholinergic neurons to better understand how cholinergic activity affects different stages of spatial memory formation in a reward-based navigation task in mice. We found that optogenetic stimulation of septal cholinergic neurons (1) impaired memory formation when activated at goal location but not during navigation; (2) reduced sharp wave-ripple incidence at goal location; and (3) reduced ripple incidence and enhanced theta-gamma oscillations during sleep. These results underscore the importance of appropriate timing of cholinergic input in long-term memory formation, which might help explain why there has been limited success of cholinesterase inhibitor drugs in the treatment of memory impairment in Alzheimer's disease.

Introduction

The role of the neuromodulator acetylcholine (ACh) in learning and memory is debated. On one hand, cholinergic neuron degeneration and a low tone of ACh correlate with memory impairment in normal and pathological ageing in humans and rodents (Bartus, 2000; Berger-Sweeney et al., 2001; Hasselmo and Sarter, 2011); indeed, drugs blocking the degradation of ACh are among the few that modestly ameliorate memory impairment in Alzheimer's disease (Ehret and Chamberlin, 2015); and extensive lesions of the medial septum (MS), where the cholinergic neurons projecting to the hippocampus are located, produce learning deficits (Hepler et al., 1985). On the other hand, selective lesions of MS cholinergic neurons, which account for ~ 5 % of neurons in the MS, have relatively little impact on learning and memory (for review see Hasselmo and Sarter, 2011; Solari and Hangya, 2018). A reason for these apparently conflicting results may lie in the fact that memory formation is a dynamic process during which ACh levels vary (Fadda et al., 2000), a property lesioning or pharmacological studies can not directly address.

In an influential model, Buzsáki (1989) suggested that long-term memory forms in two stages: first, neuronal activity produces a labile trace, then a delayed potentiation of the same synapses forms a long-lasting memory trace. He suggested that the two stages are associated with different network states of the hippocampus. In rodents, phase-amplitude-coupled theta (5–12 Hz)-gamma (30–100 Hz) oscillations (Csicsvari et al., 2003) occur during exploratory behaviors, whereas large-amplitude sharp waves combined with high-frequency ripples (SWRs) (O'Keefe and Nadel, 1978; Csicsvari et al., 2000) occur during immobility and slow-wave sleep. These two

network states are mutually exclusive (O'Keefe and Nadel, 1978; Buzsáki, 1986; Csicsvari et al., 2000) and it was suggested that memory encoding is associated with theta/gamma oscillations while memory consolidation relies on SWR activity (O'Neill et al., 2010; Colgin, 2013).

Hippocampal network states are controlled by the local release of ACh. In hippocampal CA3, cholinergic activation induces a slow gamma rhythm primarily by activating M1 muscarinic receptors (Fisahn et al., 1998; Betterton et al., 2017), while in the CA1, cholinergic activation promotes theta/gamma oscillations and suppresses ripple oscillations through the activation of M2/M4 muscarinic receptors (Vandecasteele et al., 2014; Zhou et al., 2019; Ma et al., 2020). This suggests that regulation of cholinergic tone allows the switching between online attentive processing (theta/gamma oscillations) and offline memory consolidation (SWRs) as described in the two-stage model of memory trace formation (Buzsaki, 1989). Evidence from microdialysis and electrophysiology experiments shows a high cholinergic tone during exploration, promoting theta activity, and a lower cholinergic tone during subsequent rest, permitting SWRs (Fadda et al., 2000; Giovannini et al., 2001; Fadel, 2011). Disruption of cholinergic activity at different stages of learning and memory impairs performance in memory tasks (for review see Hasselmo and Sarter, 2011; Solari and Hangya, 2018) and has improved our understanding of the dynamical aspect of cholinergic modulation. However, the differential effects of ACh in various phases of memory formation are still not well understood.

To clarify the function of the MS cholinergic system during hippocampus-dependent learning and memory, we investigated the phase-specific effect of optogenetic cholinergic stimulation in the appetitive Y-maze long-term

memory task, a simple reward-based spatial memory task with two distinctive behavioural phases: a phase of navigation towards a reward and another after arriving in the goal area (Bannerman et al., 2012). We show that increased stimulation of cholinergic neurons does not affect learning of the task when applied during navigation towards a reward, but impairs learning if stimulation is applied at the goal location. Using electrophysiological recording in both freely behaving and anesthetized mice we show that activation of MS cholinergic neurons switches the CA3 and CA1 network states from ripple activity to theta/gamma oscillations. Our recordings of hippocampal local field potential (LFP) in freely moving animals indicate that impaired memory was related to disruption of ripples, supporting the two-stage model of memory trace formation (Buzsaki, 1989).

METHODS

Animals

A total of 16 adult male wild-type (WT, C57/B6) and 51 adult male ChAT-Ai32 mice were used in this study. ChAT-Ai32 mice were bred from mice that express Cre-recombinase under the control of the choline acetyltransferase promoter (ChAT-Cre, Jackson Labs strain #006410) and mice of the Cre-reporter Ai32 line (Jackson Labs strain #012569), which carries a Cre-dependent, enhanced YFP (eYFP)-tagged channelrhodopsin-2 (ChR2)-containing expression cassette (Madisen et al., 2012). All animal experiments were performed under the Animals (Scientific Procedures) Act 1986 Amendment Regulations 2012 following ethical review by the University of Cam-

bridge Animal Welfare and Ethical Review Body (AWERB) under personal and project licenses held by the authors.

In vivo electrophysiology in anesthetized mice

Mice were anesthetized with intraperitoneal injections of 1.2 $g \cdot kg^{-1}$ urethane and their head was fixed in a stereotaxic frame. Body temperature was maintained at 35 ± 1 ^{o}C with a heating pad. The head was shaved, the Bregma and Lambda were aligned horizontally, and craniotomies were made above the MS and CA3. Simultaneous optical activation in the MS (AP: +1 mm, ML: 0 mm, DV: -3.6 mm, coordinates from Bregma) with a stripped optical fiber (200 µm, 0.22 NA; Doric Lenses) and electrical recordings in the MS or in the hippocampus (ML: +2.4 mm, AP: -2.46 mm, DV: -2.5 mm) using an extracellular parylene-C insulated tungsten microelectrode (127 µm diameter, 1 MΩ; A-M Systems) were performed.

Surgery

Surgeries were carried out following minimal standard for aseptic surgery. Mice were anesthetized with isoflurane (5% induction, 1-2% maintenance, Abbott Ltd, Maidenhead, UK) mixed with oxygen as carrier gas (flow rate 1.0-2.0 $L \cdot min^{-1}$) and placed in a stereotaxic frame (David Kopf Instruments, Tujunga, CA, USA). Then the skull was exposed after skin incision and Bregma and Lambda were aligned horizontally. A hole was drilled above the MS at coordinates AP: +1 mm and ML: 0 mm, and an optic fiber (200 µm, 0.22 NA; Doric Lenses) was lowered towards the MS (DV: -3.6 mm) at low speed (1 $mm \cdot min^{-1}$). Once positioned just above the MS, the optic fiber was

secured to the skull using dental cement (Prestige Dental).

To perform recordings in freely moving animals, we implanted 5 mice with LFP duodes, consisting of two twisted 75 µm teflon-coated silver electrodes (AGT0510, World Precision Instruments, Hitchin, UK) with tips spaced 300-500 µm, one tip being implanted in the oriens and the other tip in the pyramidal cell layer. Mice were implanted bilaterally in CA1 (AP: -1.7, ML: ±1.2, DV: 1 & 1.3) and CA3 (AP: -2.3, ML: ±2.5, DV: 1.8 & 2.1), DV being taken from the surface of the brain. Ground and reference silver wires were connected to a stainless microscrew implanted over the cerebellum: AP: - 5.3 ML: +/- 1.5. To record the electromyogram activity. a 75 µm Teflon-coated silver electrode was implanted in the neck muscle. All wires were connected to a 32 pins Omnetics connector (Genalog, Cranbrook, UK). The exposed brain was covered with a protective dura gel (Cambridge NeuroTech, UK) to prevent damage upon cementing of the electrodes. Duodes were individually glued to the skull using UV-cured glue (Tetric EvoFlow) and the implant was secured to the skull using dental cement (Super-Bond C & B; Prestige Dental, Bradford, UK). At the end of the implantation, the mice were removed from the frame, Meloxicam (2 $mg \cdot kg^{-1}$ s.c.) was administered as analgesia and animals were left to recover in a post-surgery chamber and maintained at +34.0 °C. The mice were allowed to recover for 5 days before habituation started and during these 5 days were daily monitored and given Meloxicam as an analgesic.

Appetitive Y maze task

Long-term spatial memory was assessed using the appetitive Y-maze task, as described in full by Shipton et al. (2014). Briefly, mice had to learn to find a food reward (condensed milk) on a 3-arm maze that remained at a fixed location in relation to visual cues in the room. The 3-arm maze, elevated 82 cm from the floor, consisted of gray-painted 50×13 cm arms bordered by 1 cm high white plastic walls, which extended from a central triangular platform. Plastic food wells (1.5 cm high) were positioned 5 cm from the distal end of the arms. Mice were kept on a restricted feeding schedule, allowing them to maintain at least 85% of their free food body weight. Before testing, the mice were habituated to the food reward and the maze in a different room to where behavioral testing would occur. During testing, mice were only allowed to make one arm choice each trial and were only allowed to consume the reward if the correct arm was chosen, otherwise, mice were removed from the maze and the trial was ended. Target arm assignments were counterbalanced such that at least one mouse of each experimental group was designated to each arm. Each mouse received ten trials per day for 6–10 consecutive days, five starts from the left of the target arm and five starts from the right in a pseudo-random order with no more than three consecutive starts from the left or right. The maze was rotated either clockwise or anticlockwise after each trial to discourage the use of intra-maze cues to help learn the task. Optogenetic stimulation started either from the beginning of the trial (navigation and throughout cohorts), or when the mouse reached the goal zone (goal cohort). Light stimulation ceased when the mouse reached the goal zone for the navigation cohort. Light stimulation was performed using blue laser at 473 nm (Ciel, Laser Quantum, Cheshire, UK), powered 25 ±1 mW and we used 50-ms-long pulses

at 10 Hz. Stimulation was controlled using custom made procedures in Igor Pro (WaveMetrics, Oregon, USA).

Optogenetic stimulation and electrophysiological recordings

Data were acquired from 5 ChAT-Ai32 male mice implanted with duodes for electrophysiological recordings and optic fiber for optogenetic stimulation. These mice were recorded during sleep and while performing the appetitive Y-maze task.

For recordings during sleep, after connecting the electrodes to the Whisper acquisition system (Neural Circuits, LLC, VA, USA) and optic fiber to the laser, the animals were placed in a cage (different to their home cage), to which the animal was habituated over a period of two days. The floor of the cage was covered with standard bedding. The recordings started after the mice visibly stopped moving and consisted of 30-s-long laser stimulation at 473 nm, power 25 ±1 mW using 50-ms-long pulses at 10 Hz alternating with 60-120 s interval without the stimulation. An overhead webcam camera tracked the movement and position of the animal. The videos were manually reviewed together with the recorded EMG signal to exclude trials that were interrupted by the mice moving.

For Y-maze task, the mice underwent the same habituation and learning protocol as described above in the appetitive Y-maze task section. During learning, mice were connected to the laser and to the Whisper acquisition system and placed at the starting arm of the maze. The laser was activated in the goal zone on alternating trials to allow within-subject comparison. These 5 mice were not added to the behavioral cohort as the stimulation protocol (50

% of the trials) was different from that used in behavior only (stimulation performed for all trials).

The position of the animal was tracked with an overhead webcam and automatically extracted using custom procedures in MATLAB (MATLAB, 2019. All recordings were performed using the Whisper acquisition system sampling at 25 kHz, laser stimulation was triggered using custom made procedures in Igor Pro and synchronized with the electrophysiological and webcam recordings.

Electrophysiology data analysis

Data analysis was performed in MATLAB Release 2019b (MATLAB, 2019) and R version 3.4.4 (R Core Team, 2018). To reduce contamination by volume conducted signal, we performed duode recordings. In the CA1, a single duode recorded from the oriens and the pyramidal cell layer; in the CA3, from the lacunosum moleculare and pyramidal cell layer. The duode signal was substracted, enhancing signal differences between the hippocampal layers. To remove noise artifacts caused by wire movement, changes in the consecutive samples of the EMG signal were detected. If the change exceeded a threshold set to 2 standard deviations, a 500 ms-long window of the signal centered on the noise timestamp was removed. We conducted the analysis on one duode from CA1 and one from CA3 based on the quality of signals for both theta oscillations and ripples.

For ripple detection, we adapted the method from (Vandecasteele et al., 2014). The signal was down-sampled to 1.25 kHz and 80–250 Hz band-pass filtered with Type II Chebyshev phase-preserving filter (filter order = 4,

stopband attenuation = 20 dB). Next, the filtered signal was squared, mean-subtracted, and smoothed by applying a moving average with 10-ms-long window. Ripples were detected when the squared signal crossed 2 standard deviations for 20–300 ms duration and its peak crossed 6 standard deviations in freely moving animals and 4 standard deviations in urethane-anesthetized animals. Ripple incidence was calculated as the number of detected ripples divided by the duration of the recording.

Power spectral density (PSD) was estimated using Welch's method (MATLAB built-in *pwelch* function with 0.5 s window and 0.25 s overlap) for frequencies spanning the range from 1 to 200 Hz. To visualize instantaneous changes in PSD during Y-maze trials, spectrogram was created with continuous wavelet transform using Morlet wavelets (MATLAB built-in *cwt* function with default parameters). Throughout the study, we defined theta and gamma frequency bands as the band ranging 2.5–5 Hz during anesthesia and 5–11 Hz otherwise for theta; 20–40 Hz during anesthesia and 25–45 Hz otherwise for slow gamma. The slow gamma frequency upper bound was chosen to exclude any line noise contamination at 50 Hz.

To estimate relative theta and slow gamma power, we used the FOOOF tool (https://github.com/fooof-tools/fooof) developed by Haller et al. (2018). It models the estimated PSD as the sum of background spectrum and Gaussian peaks in narrowband frequencies. The background spectrum was fitted on the PSD log-log plot with a straight line, which corresponds to a pink noise-like (1/f) background. To minimize the model error – the difference between the actual and the modeled PSD – the background spectrum fit was found in two frequency ranges separately (2 - 20 Hz and 15 - 150 Hz). Rela-

tive theta and slow gamma peaks, as well as their peak frequencies, were taken from the Gaussian peaks fitted above the background spectrum.

Statistical analysis

Statistical analysis was performed in R version 3.4.4 (R Core Team, 2018). Data are reported as mean ± SEM unless otherwise stated. For significance testing, first, the normality of the data was assessed by Shapiro-Wilk test and by inspection of the quantile-quantile plot. If the normality criterion was satisfied ($p > 0.05$), a parametric test (*t*-test) was used, otherwise a non-parametric test (one-way ANOVA on ranks or Wilcoxon test) was used, as described in the Results section.

The effects of the optogenetic manipulation on ripple incidence and other quantities in freely moving mice were assessed with linear mixed-effects models. This method allows for correlations that exist in our data between samples coming from trials repeated in the same mouse and allows for an unbalanced number of samples between mice. Laser stimulation ($L \in \{0$ *for inactive*, 1 *for active*$\}$) was a fixed effect in the model; the random variable representing the animal (*a)* was treated as a random effect in the intercept and slope estimation. The quantity *Y* in the trial *i* for animal *a* was modeled as:

$$Y_i = \beta_0 + R_{0a} + (\beta_1 + R_{1a}) * L + \varepsilon_i \text{ , where:}$$

- β_0, β_1 are linear regression coefficients for the fixed effects
- R_{0a}, R_{1a} are random effects: normally distributed animal-specific corrections for linear regression coefficients with zero mean and maximum-likelihood standard deviation estimated by the model

- ε_i is a random error with a normal distribution with zero mean and maximum-likelihood standard deviation estimated by the model.

The residual errors were checked for the assumptions of the linear models: mean of zero, no correlation with the predicted values and homoscedasticity. To satisfy these assumptions when modeling ripple duration, a log-linear model of variable *Y* was created as above.

The linear mixed-effects models were built in R with package 'lme4' and p values for the fixed effects were obtained using Sattherwaite estimation of degrees of freedom implemented in the 'lmerTest' R package.

Histological processing

Animals were terminally anesthetized by intra-peritoneal injection of pentobarbital (533 $mg \cdot kg^{-1}$) and then transcardially perfused with phosphate-buffered saline (PBS) followed by 4% paraformaldehyde (PFA). Brains were removed and post-fixed for 24–48 hours, then rinsed and subsequently cryoprotected overnight in 30% (w/v) sucrose dissolved in PBS. Coronal sections of 30–40 μm thickness of the MS to hippocampus were cut using a microtome (Spencer Lens Co., Buffalo, U.S.A.).

To verify the expression of ChR2 fused with the eYFP tag or ArchT fused with the eGFP tag and visualize the location of cholinergic neurons, sections were immunostained for eYFP/eGFP and ChAT. After rinsing in PBS, sections were incubated for 1 hour in a blocking solution comprising PBS with 0.3% (weight/volume) Triton X-100 and 5% (weight/volume) donkey serum (Abcam) containing 1% (w/v) bovine serum (Sigma). Sections were then incubated for ≥15 hours at 4 ^{o}C with chicken anti-GFP (1:1000, Abcam AB13970)

and goat anti-ChAT (1:500, Milipore AB144) antibodies. The sections were then washed, followed by 2 hours of incubation in blocking solution containing anti-chicken Alexafluor488 (1:400; Life Technologies A11039) and anti-goat Alexafluor594 (1:1000, Abcam AB150132) at room temperature. Finally, the sections were rinsed and mounted in Fluoroshield with DAPI (Sigma).

To identify the placement of the electrode (aided by DiI application) and optic fiber tracks for each mouse, sections containing evidence of the implant were selected and mounted in Fluoroshield (Sigma).

Sections were examined with a Leica Microsystems SP8 confocal microscope using the 10× and 20× magnification objectives. The eYFP$^+$/GFP$^+$ and ChAT$^+$ cells were quantified manually using the ImageJ software. The location at which the implant appeared the deepest was determined and used to plot the implant location on the corresponding section in a mouse brain atlas (Franklin and Paxinos, 2007).

Data and code availability

Code used for the analysis and to generate the figures can be accessed on the authors' GitHub site: https://github.com/przemyslawj/ach-effect-on-hpc. Electrophysiological data will be shared on any request.

RESULTS

Functional expression of ChR2 in cholinergic neurons

We aimed to investigate the effects of cholinergic modulation on hippocampal oscillations and performance in a spatial navigation task. To this end, we optogenetically controlled the activity of cholinergic neurons using ChAT-

Ai32 mice that expressed enhanced YFP-tagged channelrhodopsin-2 (ChR2-eYFP) under the control of the choline-acetyl transferase promoter (ChAT). We first checked the expression of ChR2 in MS cholinergic neurons by performing double immunostaining for ChAT and YFP (Figure 1A). Out of 111 ChAT-immunopositive neurons in the MS, 98 (83.13%, n = 3 mice) were also immunopositive for YFP (YFP^+ChAT^+). We did not detect YFP-immunopositive cells that were negative for ChAT (YFP^+ChAT^-), indicating a selective expression of ChR2-eYFP in ChAT cells.

We probed the functional expression of ChR2 in MS neurons by recording multi-unit activity in the MS of urethane-anesthetized mice. 473 nm light was delivered through an optic fiber implanted just above the MS while multi-unit activity was recorded from a co-assembled electrode whose tip protruded ~200 μm further than the optic fiber tip. Local light delivery (50 ms pulses at 10 Hz) resulted in an increase in multi-unit activity (baseline spike frequency: 7.9 ± 2.8 Hz vs. spike frequency during light delivery: 22.7 ± 7.3 Hz, two-tailed Wilcoxon matched pair signed-rank test: $p = 0.03$; n = 6 recordings from 2 mice; Figure 1B), confirming our ability to increase neuronal activity in the MS using optogenetics.

Activation of septal cholinergic neurons in the goal zone slows place learning

We investigated the effect of cholinergic activation during different phases of the appetitively-motivated Y-maze task, a hippocampus-dependent task commonly used to study long-term spatial memory (Bannerman et al., 2012; Shipton et al., 2014). Mice had to learn to find a food reward on an ele-

vated 3-arm maze that remained at a fixed location in relation to visual cues in the room, while the mice pseudo-randomly started from one of the other two arms. As short-term memory errors caused by re-entry during a single trial have previously been shown to impair the acquisition of this spatial long term memory task (Schmitt et al., 2003), mice were only allowed to make one arm choice in each trial to isolate the long-term memory process (Figure 2A). Previous studies have reported sharp wave ripples, i.e. offline processing, at the reward location of different spatial navigation tasks (O'Neill et al., 2006; Dupret et al., 2010). Based on these studies, we defined a navigation phase corresponding to the arms of the maze except for the distal ends (20 cm from the edge), which we considered as goal zones. Cholinergic activation was achieved by light stimulation (473 nm, 25 mW, 50-ms-long pulses at 10 Hz) delivered via an optic fiber implanted in the MS of ChAT-Ai32 mice. ChAT-Ai32 mice were split into four groups to test four experimental conditions: (i) no stimulation (n = 13), (ii) optogenetic stimulation during navigation – from the start of the trial until they reached the goal zone (n = 9), (iii) optogenetic stimulation in the goal zone only - from the entry of the goal zone until the mice were removed from the maze either after they had eaten the food or they had reached the empty food well (n = 15), and (iv) optogenetic stimulation throughout the maze (n = 9; Figure 2B). Mice from all four cohorts learned the task but the acquisition was slower when cholinergic neurons were activated in the goal zone (Figure 2C). To control for possible aversive effects of the illumination, we performed an additional experiment with MS-implanted wild-type (WT) mice split into 2 groups: no stimulation (n = 7) and light delivery in the goal zone (n = 9; Figure 2D).

We set a learning criterion of ≥80 % successful trials in a day. Comparison between the 6 cohorts revealed differences in reaching this criterion (one-way ANOVA on ranks $\chi^2(5) = 17$, $p = 0.005$; Figure 2E). Dunn posthoc tests indicated that the ChAT-Ai32 'goal' group was delayed at learning the task compared to the ChAT-Ai32 'no stimulation' group (4.47 ± 0.32 days vs 2.85 ± 0.25 days, $p = 0.0003$). Similarly the ChAT-Ai32 'goal' group was delayed compared to the ChAT-Ai32 'navigation' group (4.47 ± 0.32 days vs 3.11 ± 0.35 days, $p = 0.01$). Conversely we did not observe any learning difference between the 'goal' and 'no stimulation' groups in the WT mice cohorts (goal: 3.0 ± 0.37 days; no stimulation: 3.4 ± 0.37 days; $p = 0.6$).

These results suggest that cholinergic activation in the goal zone for 10–30 s slows learning of the appetitive Y-maze task. At the same time, optogenetic activation during navigation or throughout the maze had no significant effect on task acquisition. We confirmed that a long-term memory trace had formed by retesting the mice on the Y-maze task one week after the end of the acquisition period for each group of the ChAT-Ai32 mice (no stimulation: 100 ± 0 %; navigation: 99 ± 1 %; goal: 94 ± 3 %; throughout: 100 ± 0 %). After behavioral testing, implant placement and the level of eYFP expression were verified by immunohistochemistry, confirming that there were no significant differences in implant placement between the behavioral groups (Figure 2 – figure supplement 1).

Activation of medium septum cholinergic neurons reduces the incidence of ripples via muscarinic receptor activation

To gain an understanding of why activating MS cholinergic neurons in the goal zone impairs task acquisition, we performed recordings from the hippocampal CA1 and CA3 areas of freely moving mice. A previous study showed that activation of septal cholinergic neurons suppresses SWRs in hippocampal CA1 (Vandecasteele et al., 2014). Here, we investigated how the cholinergic manipulation affects both CA3 and CA1 activity (Buzsáki, 1986; Csicsvari et al., 2000; Oliva et al. 2016).

We implanted recording electrodes in the CA1 and the CA3 and the optic fiber above the MS of the ChAT-Ai32 mice. We recorded LFP signal while the mice slept in a cage, to which they were familiarized over the two previous days. Within a single behavioral session, we alternated 30-s-long epochs with the stimulation on with 60 - 120-s-long epochs without the stimulation. Only epochs when the mouse was asleep for their full duration were used for the analysis (10 ± 2 epochs per animal, n = 5 animals).

Optogenetic stimulation reduced the ripple incidence both in the CA1 and the CA3, and this reduction followed the duration of the stimulation (Figure 3A-B). To account for correlations between the epochs for the same mouse, we assessed this effect with a linear mixed-effects model (see Methods). Optogenetic stimulation significantly reduced ripple incidence in the CA1 from 0.26 ± 0.06 Hz to 0.05 ± 0.02 Hz ($F_{(1, 3.7)} = 0.24$, $p = 0.01$, n = 5 animals) and in the CA3 from 0.26 ± 0.03 Hz to 0.08 Hz ± 0.02 Hz ($F_{(1, 10)} = 41$, $p < 10^{-4}$, n = 5 animals). We did not observe any effect of the laser stimulation on ripple peak frequency (linear mixed-effects model, CA1: $F_{(1, 172)} = 1.78$, $p = 0.18$; CA3: $F_{(1, 4.3)} = 0.13$, $p = 0.73$) or ripple duration (log-linear mixed-effects model, CA1: $F_{(1, 4.4)} = 0.40$, $p = 0.56$; CA3: $F_{(1, 5)} = 0.25$, $p = 0.64$).

To investigate the mechanism by which the CA3 ripples are suppressed, we performed the same optogenetic manipulation in urethane-anesthetized mice (1.2 $g \cdot kg^{-1}$), which allowed us to combine recordings and pharmacological investigation. Under anesthesia, the ripples had an incidence of 0.24 ± 0.05 Hz (n = 7 mice) and were similar in appearance to those recorded in naturally sleeping animals: their peak frequency was 124 ± 2 Hz, compared to 132 ± 2 Hz in sleeping animals and their duration was 41 ± 2 ms compared to 33 ± 1 ms in sleeping animals. Stimulation of MS cholinergic neurons (473 nm light, 25 ms pulses, 20 Hz for 30 s) significantly reduced ripple incidence to 0.05 ± 0.03 Hz (median = 0.00 Hz; n = 7 mice; two-tailed Wilcoxon paired test: p = 0.02; Figure 3D), which was prevented by prior intra-peritoneal administration of scopolamine, a muscarinic receptor antagonist (2 $mg \cdot kg^{-1}$; control: 0.33 ± 0.03 Hz, median = 0.33 Hz; optogenetic stimulation: 0.33 ± 0.05 Hz, median = 0.29 Hz; n = 9 mice; two-tailed paired t-test: p = 0.81; Figure 3D).

Hence, our results demonstrate that optogenetic activation of MS cholinergic neurons suppresses ripple incidence both in the CA1 and in the CA3 where we confirmed that the suppression occurs through the activation of muscarinic receptors.

MS cholinergic neurons increased theta and slow gamma activity in sleeping animals

We next investigated the effect of optogenetic stimulation of MS cholinergic neurons on the other hippocampal network state: theta-gamma activity in the sleeping mouse.

We determined the power spectral density for frequencies ranging 1 - 200 Hz in control and during stimulation. We observed a reduction of the power spectral density (PSD) across the full frequency range upon light stimulation (Figure 4B-C, Figure 4 – figure supplement 1), as reported previously (Vandecasteele et al., 2014). PSD from electrophysiological recordings are the summation of a periodic signal and a background spectrum that is greatly influenced by aperiodic activity whose intensity on PSD is of pink noise (1/f) (Haller et al., 2018). Therefore, to quantify the power of theta and gamma oscillations, we estimated the background spectrum and looked at the relative peaks in the PSD above the fitted background spectrum (Haller et al., 2018, see Methods, Figure 4C).

Background spectrum intensity decreased with light stimulation (linear fixed-effects model on background spectrum area under curve (AUC) on PSD log log plot, CA1: AUC decreased from -5.96 ± 0.05 to -6.21 ± 0.06, $F_{(1, 4)}$ = 46, p = 0.004; CA3: AUC decreased from -6.07 ± 0.02 to -6.20 ± 0.04 $F_{(1, 8)}$ = 87, $p < 10^{-5}$; Figure 4D). Even though theta power was low during sleep outside of REM sleep, in the CA1, 93 ± 7 % of the control and 95 ± 5% of the stimulated epochs had a peak in the theta band of a higher power than the background spectrum estimated at that frequency (relative theta peak); in the CA3, 99 ± 1 % of control and 100 ± 0 % of stimulated epochs had a relative theta peak. During optogenetic stimulation, theta power relative to fitted background spectrum significantly increased in the CA1 by 34 ± 8 % and in the CA3 by 21 ± 8 % (linear fixed-effects model, CA1: $F_{(1, 44)}$ = 16, p = 0.0002; CA3: $F_{(1, 6)}$ = 8, p = 0.03, n = 5 animals). The increase in the power was associated with significantly lower frequency of the theta peak in the CA1 but not

in the CA3 (linear mixed-effects model, change in the CA1 from 7.9 ± 0.1 Hz to 7.2 ± 0.2 Hz, $F_{(1, 5)} = 16$, $p = 0.01$; change in the CA3 from 7.6 ± 0.2 to 7.1 ± 0.2 Hz; CA3: $F_{(1, 5)} = 4$, $p = 0.11$). The stimulation also enhanced oscillations in the slow gamma band (25 - 45 Hz) and the slow gamma power relative to fitted background spectrum (relative slow gamma) increased in the CA1 by 54 ± 6 % and in the CA3 by 8 ± 8 % (linear fixed-effects model, CA1: $F_{(1, 4)} = 24$, $p = 0.01$; CA3: $F_{(98, 5)}$, $p = 0.02$), while the peak frequency did not significantly change from 39 ± 1 Hz in the CA1 and 38 ± 2 Hz in the CA3 (linear mixed-effects model, CA1: $F_{(1, 5)} = 0.2$, $p = 0.64$; $F_{(1, 90)} = 0.51$, CA3: $p = 0.48$).

Similar results were obtained from anesthetized mouse recordings. Optogenetic stimulation significantly increased the CA3 relative theta power (2.5 – 5 Hz, Wilcoxon signed-rank test, $V = 0$, $p = 0.04$, $n = 7$ mice) and the relative slow gamma power (Wilcoxon signed-rank test, $V = 1$, $p = 0.03$, $n = 7$ mice), an effect that was prevented by injecting of the muscarinic antagonist scopolamine (relative theta power: Wilcoxon signed-rank test, $V = 15$, $p = 0.40$; relative slow gamma power: Wilcoxon signed-rank test, $V = 34$, $p = 0.20$, $n = 9$ mice; Figure 4 – figure supplement 2).

Thus our results demonstrate that in sleeping and urethane-anesthetized mice, optogenetic stimulation of MS cholinergic neurons promotes theta-gamma oscillations in the CA1 and the CA3 primarily via activation of muscarinic receptors.

Activation of septal cholinergic neurons in the goal zone slows place learning by reducing CA1 ripple incidence and CA3 slow gamma.

We last asked how the oscillatory regimes vary during the appetitive Y maze and how ACh neuron stimulation modulate the oscillations in the goal zone. To investigate whether the changes in the ripple activity and theta-gamma oscillations are responsible for the impaired place learning, we performed the Y-maze task using the same ChAT-Ai32 mice (n = 4) implanted with recording electrodes and the optic fiber. Optogenetic stimulation was applied when the mouse reached the goal zone (Figure 5A) on alternating trials, allowing us to compare the CA1 and the CA3 activity between the stimulated and non-stimulated trials. Mice were trained and recorded over 6 days, and by day 5 had reached 70 ± 10 % successful trials. We analyzed only the successful trials (14 ± 2 trials per animal with no stimulation and 11 ± 1 trials with the stimulation at goal zone). SWR in CA1 and CA3 occurred at start and goal locations (Figure 5B-C) and optogenetic stimulation significantly reduced the ripple incidence at goal in the CA1 from 0.12 ± 0.02 Hz to 0.06 ± 0.01 Hz. However, light did not significantly affect ripple incidence in CA3 (0.12 ± 0.02 Hz; linear mixed-effects model, CA1: $F_{(1, 5.7)} = 6.72$, $p = 0.04$; CA3: $F_{(1, 10)} = 0.06$, $p = 0.81$, n = 3 mice included in the analysis with ripple incidence at goal ≥ 0.03 Hz). The ripple incidence in the non-stimulated epochs was not significantly different between the early (before day 5) and late learning (linear mixed-effects model, CA1: $F_{(1, 8.9)} = 2.1$, $p = 0.18$; CA3: $F_{(1, 6.6)} = 0.01$, $p = 0.74$, n = 3 mice).

The mouse behavior strongly modulated hippocampal activity. We recorded the highest theta power intensity in the central section of the maze where the mice run the fastest (Figure 5E) while at the goal location, where the mice consumed the reward, theta (5 – 11 Hz) and high gamma frequency

bands (80 – 200 Hz) showed reduced power intensity (Figure 5E, right panel). Nevertheless, theta and slow gamma bands peaked above the background spectrum at the goal location in the control trials (88 ± 12% of trials had a theta peak in the CA1 signal and 85 ± 12 % in the CA3; 98 ± 1 % trials had a slow gamma peak in the CA1 signal and 88 ± 10 % in the CA3, Figure 5F). Delivering light did not affect the relative theta power intensity (linear fixed-effects model, CA1: $F_{(1, 2.8)} = 0.01$, $p = 0.94$; CA3: $F_{(1, 3.7)} = 0.04$, $p = 0.84$, Figure 5H), neither did it affect the relative slow gamma power in CA1 at the goal location. However, we observed a 15 ± 4 % increase of slow gamma power intensity in the CA3 when light was applied (linear fixed-effects model, CA1: $F_{(1, 2.8)} = 4.1$, $p = 0.14$; CA3: $F_{(1, 23)} = 5.2$, $p = 0.03$, Figure 5I).

Overall, these results show that optogenetic stimulation of MS cholinergic neurons reduces ripple incidence in the CA1 and increases slow gamma power intensity in the CA3. Hence this suggests a causal relationship between the ripple incidence at the goal location and memory formation and highlights the need of a timely control of ACh release in the hippocampus during learning.

DISCUSSION

Using optogenetics, we investigated the effects of stimulating MS cholinergic neurons on hippocampal LFPs and memory when delivered at different phases of an appetitively-motivated spatial memory task. We found that (1) MS cholinergic activation at the goal location, but not during navigation, impairs spatial memory formation; (2) MS cholinergic stimulation during reward con-

sumption reduces ripples incidence in the CA1 and promotes slow gamma in the CA3; and (3) cholinergic stimulation reduces hippocampal ripple incidence and promotes theta-gamma rhythm in both the CA1 and the CA3 in the sleeping mouse. These results show that timely control of cholinergic modulation is crucial for spatial learning on a time scale of seconds. Moreover, our results indicate that cholinergic stimulation suppresses ripple activity in both sleeping and awake, behaving animals, explaining the learning deficit induced by inappropriately timed cholinergic activity.

Cholinergic influence on hippocampal network activity

The correlation between hippocampal network activity and cholinergic tone or MS cholinergic neuron activity is well established. MS cholinergic neurons discharge at a maximal rate when the animal is running (Ma et al., 2020), which corresponds to highest theta power intensity in the CA1 and highest cholinergic tone measured in the pyramidal layer of CA1 (Fadda et al., 2000; Fadel, 2011). Conversely, cholinergic tone and MS cholinergic neuron discharge is at its lowest during slow wave sleep and wake immobility, which are associated with the highest ripple incidence (Fadda et al., 2000; Ma et al. 2020).

In accordance with these observations, we found that stimulation of MS cholinergic neurons strongly reduces ripple activity in both naturally sleeping and anesthetized animals, consistent with previous reports (Figure 3; Vandecasteele et al., 2014; Zhou et al., 2019; Ma et al., 2020). However, MS cholinergic stimulation did not significantly reduce the ripple occurrence in the CA3 when the mouse was in the goal zone of the Y-maze, while the incidence de-

creased in the CA1 (Figure 5). The lack of significant ripple incidence reduction in CA3 in the behaving mouse could be due to ripple detection failure or low numbers of animals tested but this seems unlikely as the same mice were used for sleep recording, during which ripple incidence reduction was observed upon light stimulation (Figure 3). Thus, it is possible that MS cholinergic stimulation differentially affects ripple induction or propagation depending on the mouse behavioral state. Interestingly, hippocampal area CA2 has recently been suggested to be crucial for initiating SWRs in awake mice (Oliva et al., 2016; Alexander et al., 2018), while both CA2 and CA3 could initiate them in sleeping animals, providing a possible explanation for this finding.

We show that stimulation of MS cholinergic neurons promotes theta-gamma rhythm in the CA3 and CA1 of sleeping and anesthetized animals, consistent with previous findings in the CA1 (Figure 4; Vandecasteele et al., 2014; Zhou et al., 2019; Ma et al., 2020). Similar to the report by Vandecasteele et al. (2014), only mild effects of MS cholinergic stimulation on theta and gamma peak power were seen in the sleeping mouse (Figure 3) due to a global reduction of the background aperiodic signal (1/f) also observed in Vandecasteele et al. (2014). However, the peak relative to the fitted background (Haller et al., 2018) revealed an increase in rhythmic theta-gamma power intensity (Figure 3 and 5).

Pharmacological evidence *in vivo* indicates the presence of two distinct mechanisms of theta oscillations in the hippocampus, an atropine-sensitive and an atropine-resistant component (Petsche et al., 1962; Buzsáki, 2002; Colgin, 2013). The atropine-sensitive component is mediated by the combination of cholinergic and GABAergic neurons in the MS (Buzsáki, 2002;

Manseau et al., 2008) and is slower than the atropine-insensitive theta rhythm, which is generated primarily by the entorhinal cortex (Buzsáki, 2002; Colgin, 2013). Moreover, atropine-sensitive theta was best detected in the anesthetized animal while atropine-insensitive theta was shown to predominate in the running animal (Kramis et al., 1975; Newman et al., 2013). Consistent with this division, MS cholinergic stimulation enhanced a scopolamine-sensitive theta oscillation in both anesthetized and sleeping mice (supplementary Figure 3) and shifted theta peak to a lower frequency in sleeping mice (Figure 3), while theta power intensity was not affected by MS cholinergic stimulation in the behaving mouse (Figure 5). The weak effect of MS cholinergic stimulation on theta-gamma rhythm in awake animals during the memory task could be explained either by the prominence of an atropine-resistant entorhinal-driven theta that would override any atropine-sensitive theta or, alternatively or additionally, by an already maximal cholinergic tone. Interestingly, we did observe an increase of slow gamma power in the CA3 of the behaving mouse but not in the CA1 (Figure 5). This is likely due to the activation of the recurrent connections in the CA3, leading to a more prominent increase of the spectral power.

Importance of timely regulation of cholinergic tone for memory formation

We found that temporally controlled optogenetic stimulation of MS cholinergic neurons could affect learning of the appetitive Y-maze task. Stimulation of the cholinergic neurons during navigation had no effect on the mouse perfor-

mance while, strikingly, cholinergic stimulation in the goal zone significantly impaired task acquisition (Figure 2).

The lack of behavioral effect of light stimulation during the navigation phase, when the cholinergic tone is naturally high (Fadda et al., 2000; Giovannini et al., 2001; Fadel, 2011), may suggest that release of ACh in the hippocampus is already maximal, or that ACh receptors are saturated. MS cholinergic neurons are slow spiking neurons with a maximal rate of ~ 10 Hz during active exploration (Ma et al., 2020), which was the stimulation frequency used here. It is plausible that the ACh concentration in the hippocampus might have already reached a plateau naturally, on top of which our stimulation protocol would not permit a further increase.

The impairment of memory formation by cholinergic stimulation in the goal zone, when the cholinergic tone is naturally lower (Fadda et al., 2000; Giovannini et al., 2001; Fadel, 2011), suggests that any potential beneficial effect of increased excitability or synaptic plasticity is outweighed by a requirement of reduced cholinergic activity. There is evidence to suggest that CA1 SWRs, which occur during low cholinergic activity, play a crucial role in memory formation (Ego-Stengel and Wilson, 2010; Girardeau et al., 2004; Jadhav et al., 2012; Roux et al., 2017): disruption of SWRs in the first 15 to 60 minutes following training impairs learning of spatial navigation tasks (Ego-Stengel and Wilson, 2010; Jadhav et al., 2012). In exploring animals, SWRs occur during transient immobility periods, including periods at goal locations (O'Neill et al., 2006; Dupret et al., 2010; Roux et al., 2017). These SWRs stabilize spatial representations of the CA1 place cells supporting navigation towards the newly learned goals (Roux et al., 2017), and are predictive of performance in

a spatial memory task (O'Neill et al., 2006; Dupret et al., 2010). During these SWRs, sequences of neuronal activation are replayed in reverse order with the activation first of cells whose place fields are close to the animal (Foster and Wilson, 2006; Csicsvari et al., 2007; Diba and Buzsáki, 2007; Karlsson and Frank, 2009; Ambrose et al., 2016). In contrast, SWRs occurring outside of the learning environment are not triggered by sensory stimuli, and sequences of cell activation are usually played in the forward direction (Diba and Buzsáki, 2007). These latter SWRs have been more studied and a series of experiments disrupting their occurrence have shown they are crucial for memory formation (Ego-Stengel and Wilson, 2010; Girardeau et al., 2004; Jadhav et al., 2012). We found that MS cholinergic activation for the brief time the mice spent in the reward zone, shorter than 30 s, is sufficient to significantly impair memory formation in the Y-maze task (Figure 2) likely to be caused by the disruption of SWR activity in CA1 (Figure 3). This might suggest that the reverse replay of cell sequence in the reward zone is important for learning. However, additional effects of MS cholinergic activation on intracellular signaling cascades and synaptic plasticity (Brzosko et al., 2019) or synaptic inhibition can not be ruled out at this stage (Hasselmo and Sarter, 2011; Haam and Yakel, 2017).

Possible implications for neurodegenerative disorders

Loss of cholinergic neurons in the basal forebrain is one of the hallmarks of AD (Whitehouse et al., 1982; Bowen et al., 1982), which is also associated with a reduction of ACh transporter expression in most cortical and subcortical areas (Davies and Maloney, 1976). These observations have led to the

cholinergic hypothesis of AD, which suggests that loss of cholinergic inputs plays a role in the cognitive impairment of AD patients. However the association between the loss of basal forebrain cholinergic neurons and AD is not completely clear (Mesulam, 2004), and a growing body of anatomical and functional studies suggests that MS cholinergic neuronal loss occurs in both healthy ageing and AD brain (Schliebs and Arendt, 2011; Hampel et al., 2018). Therefore, drugs compensating for the decline of cholinergic tone are seen as a rational treatment of both ageing-related memory loss and AD. However, so far, drugs targeting the cholinergic systems have shown limited beneficial effects on cognitive deficits of ageing and AD but the reason why is not entirely clear (Farlow et al., 2010; Ehret and Chamberlain, 2015). Our results shed some light on why cholinergic drugs have largely failed to improve the cognitive impairments in AD. Cholinesterase inhibitors prolong cholinergic activity by ~100 times and increase the basal cholinergic tone in the absence of spontaneous activity (Hay et al., 2015). In rodents, cholinergic tone is high during exploration, which maintains the 'online' hippocampal state dominated by theta and gamma oscillations (Buzsáki, 1989; Fadda et al., 2000; Giovannini et al., 2001). It is possible that cholinesterase inhibitors maintain a high cholinergic tone, preventing the network from transitioning into a SWR-dominant state. This could impair memory formation as our results suggest that artificially increasing ACh release for as short a time as 10-30 s during a low-cholinergic state is sufficient to impair task acquisition (Figure 2). Moreover, enhancement of cholinergic activity during the 'online' state did not bring beneficial effects to memory formation. Thus, our results suggest that suboptimal timing of cholinergic activity impairs long-term memory formation and sup-

ports the idea that appropriate timing of cholinergic modulation is crucial in learning and memory (Micheau and Marighetto, 2011).

REFERENCES

Alexander GM, Brown LY, Farris S, Lustberg D, Pantazis C, Gloss B, Plummer NW, Jensen P, Dudek SM (2018) CA2 neuronal activity controls hippocampal low gamma and ripple oscillations. Elife 7:e38052.

Ambrose RE, Pfeiffer BE, Foster DJ (2016) Reverse replay of hippocampal place cells is uniquely modulated by changing reward. Neuron 91(5): 1124-1136.

Bannerman DM, Bus T, Taylor A, Sanderson DJ, Schwarz I, Jensen V, Hvalby Ø, Rawlins JNP, Seeburg PH, Sprengel R (2012) Dissecting spatial knowledge from spatial choice by hippocampal NMDA receptor deletion. Nat Neurosci 15(8):1153-1159.

Bartus R (2000) On neurodegenerative diseases, models and treatment strategies: lessons learned and lessons forgotten a generation following the cholinergic hypothesis. Exp Neurol 163:495–529.

Berger-Sweeney J, Stearns NA, Murg SL, Floerke-Nashner LR, Lappi DA, Baxter MG (2001) Selective immunolesions of cholinergic neurons in mice: effects on neuroanatomy, neurochemistry, and behavior. J Neurosci 21(20): 8164-8173.

Betterton RT, Broad LM, Tsaneva-Atanasova K, Mellor JR (2017) Acetylcholine modulates gamma frequency oscillations in the hippocampus by activation of muscarinic M1 receptors. Eur J Neurosci 45(12):1570-1585.

Bowen DM, Benton JS, Spillane JA, Smith CC, Allen SJ (1982) Choline acetyltransferase activity and histopathology of frontal neocortex from biopsies of demented patients. J Neurol Sci 57(2-3):191-202.

Brzosko Z, Mierau SB, Paulsen O (2019) Neuromodulation of spike-timing-dependent plasticity: Past, present, and future. Neuron 103(4):563-581.

Buzsáki G (1986) Hippocampal sharp waves: their origin and significance. Brain Res 398:242–252.

Buzsáki G (1989) Two-stage model of memory trace formation: a role for "noisy" brain states. Neuroscience 31(3):551-570.

Buzsáki G (2002) Theta oscillations in the hippocampus. Neuron 33(3): 325-540.

Colgin LL (2013) Mechanisms and functions of theta rhythms. Annu Rev Neurosci 36:295-312.

Csicsvari J, Hirase H, Mamiya A, Buzsáki G (2000) Ensemble patterns of hippocampal CA3-CA1 neurons during sharp wave-associated population events. Neuron 28(2):585-594.

Csicsvari J, Jamieson B, Wise KD, Buzsáki G (2003) Mechanisms of gamma oscillations in the hippocampus of the behaving rat. Neuron 37(2):311-322.

Csicsvari J, O'Neill J, Allen K, Senior T (2007) Place-selective firing contributes to the reverse-order reactivation of CA1 pyramidal cells during sharp waves in open-field exploration. Eur J Neurosci. 26(3):704-716.

Davies P, Maloney AJ (1976) Selective loss of central cholinergic neurons in Alzheimer's disease. Lancet 2(8000):1403.

Diba K, Buzsáki G (2007) Forward and reverse hippocampal place-cell sequences during ripples. Nat Neurosci 10:1241-1242.

Dupret D, O'Neill J, Pleydell-Bouverie B, Csicsvari J (2010) The reorganization and reactivation of hippocampal maps predict spatial memory performance. Nat Neurosci 13(8):995-1002.

Ego-Stengel V, Wilson MA (2010) Disruption of ripple-associated hippocampal activity during rest impairs spatial learning in the rat. Hippocampus 20(1):1-10.

Ehret MJ, Chamberlin KW (2015) Current practices in the treatment of Alzheimer disease: Where is the evidence after the phase III trials? Clin Ther 37(8):1604-1616.

Fadda F, Cocco S, Stancampiano R (2000) Hippocampal acetylcholine release correlates with spatial learning performance in freely moving rats. NeuroReport 10:2265-2269.

Fadel JR (2011) Regulation of cortical acetylcholine release: insights from in vivo microdialysis studies. Behav Brain Res 221(2):527-536.

Farlow MR, Salloway S, Tariot PN, Yardley J, Moline ML, Wang Q, Brand-Schieber E, Zou H, Hsu T, Satlin A (2010) Effectiveness and tolerability of high-dose (23 mg/d) versus standard-dose (10 mg/d) donepezil in moderate to severe Alzheimer's disease: A 24-week, randomized, double-blind study. Clin Ther 32(7):1234-1251.

Fisahn A, Pike FG, Buhl EH, Paulsen O (1998) Cholinergic induction of network oscillations at 40 Hz in the hippocampus in vitro. Nature 394(6689):186-189.

Foster DJ, Wilson MA (2006) Reverse replay of behavioral sequences in hippocampal place cells during the awake state. Nature 440:680-683.

Franklin KBJ, Paxinos G (2007) The mouse brain in stereotaxic coordinates. third edn Academic Press. New York, NY: Elsevier Inc.

Giovannini MG, Rakovska A, Benton RS, Pazzagli M, Bianchi L, Pepeu G (2001) Effects of novelty and habituation on acetylcholine, GABA, and glutamate release from the frontal cortex and hippocampus of freely moving rats. Neuroscience 106:43-53.

Girardeau G, Benchenane K, Wiener SI, Buzsáki G, Zugaro MB (2009) Selective suppression of hippocampal ripples impairs spatial memory. Nat Neurosci 12(10):1222-1223.

Haam J, Yakel JL (2017) Cholinergic modulation of the hippocampal region and memory function. J Neurochem 142 Suppl 2:111-121.

Haller M, Donoghue T, Peterson E, Varma P, Sebastian P, Gao R, Noto T, Knight RT, Shestyuk A, Voytek B (2018) Parameterizing neural power spectra. bioRxiv. doi:10.1101/299859

Hampel H, Mesulam MM, Cuello AC, Farlow MR, Giacobini E, Grossberg GT, Khachaturian AS, Vergallo A, Cavedo E, Snyder PJ, Khachaturian ZS (2018) The cholinergic system in the pathophysiology and treatment of Alzheimer's disease. Brain 141:1917-1933.

Hasselmo ME, Sarter M (2011) Modes and models of forebrain cholinergic neuromodulation of cognition. Neuropsychopharmacology 36:52-73.

Hay YA, Lambolez B, Tricoire L (2016) Nicotinic transmission onto layer 6 cortical neurons relies on synaptic activation of non-α7 receptors. Cereb Cortex 26(6):2549-2562.

Hepler DJ, Wenk GL, Cribbs BL, Olton DS, Coyle JT (1985) Memory impairments following basal forebrain lesions. Brain Res 346(1):8-14.

Jadhav SP, Kemere C, German PW, Frank LM (2012) Awake hippocampal sharp-wave ripples support spatial memory. Science 336(6087):1454-1458.

Karlsson MP, Frank LM (2009) Awake replay of remote experiences in the hippocampus. Nat Neurosci 12(7):913-918.

Kramis R, Vanderwolf CH, Bland BH (1975) Two types of hippocampal rhythmical slow activity in both the rabbit and the rat: relations to behavior and effects of atropine, diethyl ether, urethane, and pentobarbital. Exp Neurol 49(1 Pt 1):58-85.

Li X, Yu B, Sun Q, Zhang Y, Ren M, Zhang X, Li A, Yuan J, Madisen L, Luo Q, Zeng H, Gong H, Qiu Z (2018) Generation of a whole-brain atlas for the cholinergic system and mesoscopic projectome analysis of basal forebrain cholinergic neurons. Proc Natl Acad Sci USA 115(2):415-420.

Ma X, Zhang Y, Wang L, Li N, Barkai E, Zhang X, Lin L, Xu J (2020) The firing of theta state related septal cholinergic neurons disrupt hippocampal ripple oscillations via muscarinic receptors. J Neurosci 40(18):3591-3603.

Madisen L, Mao T, Koch H, Zhuo Jm, Berenyi A, Hsu YwA, Iii AJG, Gu X, Zanella S, Gu H, Mao Y, Hooks BM, Boyden ES, Buzsáki G, Ramirez JM, Jones AR, Svoboda K, Han X, Turner EE and Zeng H (2012) A toolbox of Cre-dependent optogenetic transgenic mice for light-induced activation and silencing. Nat Neurosci 15(5):793-802.

Manseau F, Goutagny R, Danik M, Williams S (2008) The hippocamposeptal pathway generates rhythmic firing of GABAergic neurons in the medial septum and diagonal bands: an investigation using a complete septohippocampal preparation in vitro. J Neurosci 28(15):4096-107.

MATLAB, Release 2019b, The MathWorks, Inc., Natick, Massachusetts, United States.

Mesulam M (2004) The cholinergic lesion of Alzheimer's disease: pivotal factor or side show? Learn Mem 11(1):43-49.

Micheau J, Marighetto A (2011) Acetylcholine and memory: A long, complex and chaotic but still living relationship. Behav Brain Res 221(2):424-429.

Newman EL, Gillet SN, Climer JR, Hasselmo ME (2013) Cholinergic blockade reduces theta-gamma phase amplitude coupling and speed modulation of theta frequency consistent with behavioral effects on encoding. J Neurosci 33(50):19635-19646.

O'Keefe J, Nadel L (1978) The Hippocampus as a Cognitive Map. Oxford, UK: Oxford Univ Press.

O'Neill J, Senior T, Csicsvari J (2006) Place-selective firing of CA1 pyramidal cells during sharp wave/ripple network patterns in exploratory behavior. Neuron 49(1):143-155.

O'Neill J, Pleydell-Bouverie B, Dupret D, Csicsvari J (2010) Play it again: reactivation of waking experience and memory. Trends Neurosci 33(5):220-229.

Oliva, A., Fernández-Ruiz, A., Buzsáki, G. & Berényi, A. (2016) Role of hippocampal CA2 region in triggering sharp-wave ripples. Neuron 91:1342–1355.

Petsche H, Stumpf C, Gogolák G (1962) The significance of the rabbit’s septum as a relay station between midbrain and the hippocampus: I. The con-

trol of hippocampus arousal activity by the septum cells. Electroencephalogr Clin Neurophysiol 14:202-211.

R Core Team (2018). R: A language and environment for statistical computing. R Foundation for Statistical Computing, Vienna, Austria. URL http://www.R-project.org/

Roux L, Hu B, Eichler R, Stark E, Buzsáki G (2017) Sharp wave ripples during learning stabilize the hippocampal spatial map. Nat Neurosci 20:845-853.

Schliebs R, Arendt T (2011) The cholinergic system in aging and neuronal degeneration. Behav Br Res 221:555-563.

Schmitt WB, Deacon RMJ, Seeburg PH, Rawlins JNP, Bannerman DM (2003) A within-subjects, within-task demonstration of intact spatial reference memory and impaired spatial working memory in glutamate receptor-A-deficient mice. J Neurosci 23(9):3953-3958.

Shipton OA, El-Gaby M, Apergis-Schoute J, Deisseroth K, Bannerman DM, Paulsen O Kohl MM (2014) Left-right dissociation of hippocampal memory processes in mice. Proc Natl Acad Sci USA 111(42):15238-15243.

Solari N, Hangya B (2018) Cholinergic modulation of spatial learning, memory and navigation. Eur J Neurosci 48(5):2199-2230.

Vandecasteele M, Varga V, Berényi A, Papp E, Barthóc P, Venance L, Freund TF, Buzsáki G (2014) Optogenetic activation of septal cholinergic neurons suppresses sharp wave ripples and enhances theta oscillations in the hippocampus. Proc Natl Acad Sci USA 111(37):13535-13540.

Whitehouse PJ, Price DL, Struble RG, Clark AW, Coyle JT, Delon MR (1982) Alzheimer's disease and senile dementia: loss of neurons in the basal forebrain. Science 215:1237–1239.

Zhou H, Neville KR, Goldstein N, Kabu S, Kausar N, Ye R, Nguyen TT, Gelwan N, Hyman BT, Gomperts SN (2019) Cholinergic modulation of hippocampal calcium activity across the sleep-wake cycle. Elife 8:e39777.

FIGURES

FIGURE 1

ChAT-Ai32 mice express ChR2-eYFP selectively in cholinergic cells. (Ai) Overlay of DAPI, ChAT and eYFP-positive immunostaining in a coronal section of the medial septum (MS) in a ChAT-Ai32 mouse. Scale bar: 500 μm. VDB, ventral diagonal band. **(Aii-v)**: higher magnification of the MS (rectangle in **Ai**), triple immunostaining of DAPI (blue, **ii**), ChAT (red, **iii**) and eYFP (green, **iv**), showing their colocalization (overlay, **v**). Scale bar: 50 μm. **(B)** Sample trace of the recording. Top: the stimulation protocol (blue) beginning at 15 s. Inset shows a section of the 50 ms-long square stimulation pulses at 10 Hz. Middle: an example recording trace; inset shows an example unit recorded. Bottom: mean spike frequency (n = 6). *p = 0.03, two-tailed Wilcoxon matched pair signed-rank test. Gray lines represent SEM.

FIGURE 2

Cholinergic stimulation in the goal zone slows learning of the appetitive Y-maze task. (A) Mice were trained on an elevated 3-arm maze to find a food reward (red dot) in an arm that remained at a fixed location relative to visual cues in the room. Mice were allowed to consume the reward if they chose the correct arm, but were removed from the maze if they chose the incorrect arm. **(B)** Mice were pseudo-randomly split into four groups to test four optogenetic stimulation conditions. Blue indicates stimulation for the four conditions; i: no stimulation, ii: stimulation only until the goal zone is reached (gray line), iii: stimulation only in goal zone and iv: stimulation throughout the maze. **(C)** ChAT-Ai32 mice received blocks of 10 trials each day for seven consecutive days and the number of correct arm entries was recorded. The performance

of all four groups of mice improved with time but at different rates. **(D)** The same as in (C) but for WT mice. **(E)** The number of days required for each group to reach the learning criterion of ≥80%. Horizontal bars indicate the median within each group.

FIGURE 3

Activation of medium septum cholinergic neurons reduces the incidence of ripples via muscarinic receptor activation. (A) LFP recording in the CA1 and the CA3 from a sleeping mouse recorded before and during optogenetic stimulation. The trace filtered at 80–250 Hz for ripple detection is presented below. The insets show examples of the ripples marked in the original trace by dotted rectangles. **(B)** Histogram of ripple incidence before, during and after 30 s of stimulation with 50-ms-long pulses at 10 Hz (n = 64 trials from 5 mice). **(C)** Change in the ripple incidence between the stimulated and non-stimulated epochs. Lines show mean change for individual mice, ribbons extend ± 1 SEM. **(D)** Change in the ripple incidence in urethane-anesthetized mice and scopolamine (scp) injected mice prior to the recording (control: n = 7, scopolamine n = 9 mice)**.**

FIGURE 4

Cholinergic stimulation increased theta and slow gamma activity in sleeping mice. (A) LFP recording from the CA1 of a sleeping mouse recorded without (left) and with (right) optogenetic stimulation. **(B)** Mean power spectral density (PSD) of the LFP recorded from a single animal during the epochs without and with optogenetic stimulation. Gray background marks the

extent of theta and slow gamma bands. The dashed lines show a fitted background spectrum. **(C)** Inset of (B) shows PSD peaks in the theta band. Non-stimulated PSD gives the appearance of higher theta power than the stimulated PSD. This is due to a shift in the background spectrum, which can be caused by a change in the LFP noise or in the aperiodic activity and does not track the oscillatory power. The relative peak values in the PSD were used to assess the oscillatory signal. **(D)** Optogenetic stimulation shifted the background spectrum downwards, as demonstrated by a significant reduction of the area under the curve (AUC) of the fitted background spectrum for frequencies 20 – 150 Hz. **(E)** Optogenetic stimulation increased relative theta power and **(F)** gamma power. Lines show means for individual animals, ribbons extend ± 1 SEM.

FIGURE 5

Cholinergic stimulation during the Y-maze task reduced the CA1 ripple incidence and CA3 slow gamma. (A) Schematic showing the maze zones. **(B)** Example LFP and the same trace after 80 - 250 Hz filtering with a CA1 and a CA3 ripple recorded at Goal. **(C)** Time of ripples recorded in one mouse over multiple trials on one day. At Start, shows time from the trial start, at goal, shows time elapsed from the arrival at goal zone. Stimulated and non-stimulated trials are grouped together for clarity. **(D)** Change in ripple incidence at goal between the non-stimulated trials stimulated at Goal trials. **(E)** Day-mean spectrogram of the LFP recorded in the CA1, data for successful non-stimulated trials of one mouse. The values were z-scored to show relative changes in frequency. To apply the day-mean, the periods at Start and Center were

compressed or stretched to a fixed length. Right: mean z-score value at Center and Goal as a function of frequency. **(F)** Mean PSD of the LFP recorded from a single animal on non-stimulated successful trials and stimulated at Goal successful trials. Gray background marks the extent of theta and slow gamma bands. The dashed lines show a fitted background spectrum. Ribbons extend ± 1 SEM. **(G)** Change in the AUC of the fitted background spectrum, **(H)** relative theta power, and **(I)** relative slow gamma power. Lines connect means for individual animals in non-stimulated successful trials and stimulated at Goal successful trials, ribbons extend ± 1 SEM.

FIGURE 2 - Supplement 1

Implant placement did not vary between experimental groups. After behavioral testing, brains were fixed and sliced, and the placement of the deepest point of the implant was recorded for each mouse. **(A)** Representative bright field image of the optical implant site over the medial septum. Scale bar: 500 μm. **(B)** The approximate locations of the fiber optic implant tip for each mouse.

FIGURE 4 – Supplement 1

Mean PSD of the LFP recorded from each animal during sleep epochs without and with optogenetic stimulation. Gray background marks the extent of theta and slow gamma bands. The dashed lines show fitted background spectrum.

FIGURE 4 – Supplement 2

(A) Example PSD of the LFP recorded from CA3 of urethane-aneasthetised mouse. Shows separate PSD for epochs without and with optogenetic stimulation. Left: Control trial in Ach-Ai32, Right: trial after prior injection of scopolamine. The drop of power around 50 Hz is caused by notch filter applied to remove line noise. **(B)** Change in background spectrum AUC, **(C)** relative theta power, and **(D)** slow gamma power between epochs without and with stimulation. Lines connect values for individual animals (control: n = 7, scopolamine: n = 9).

Figure 1

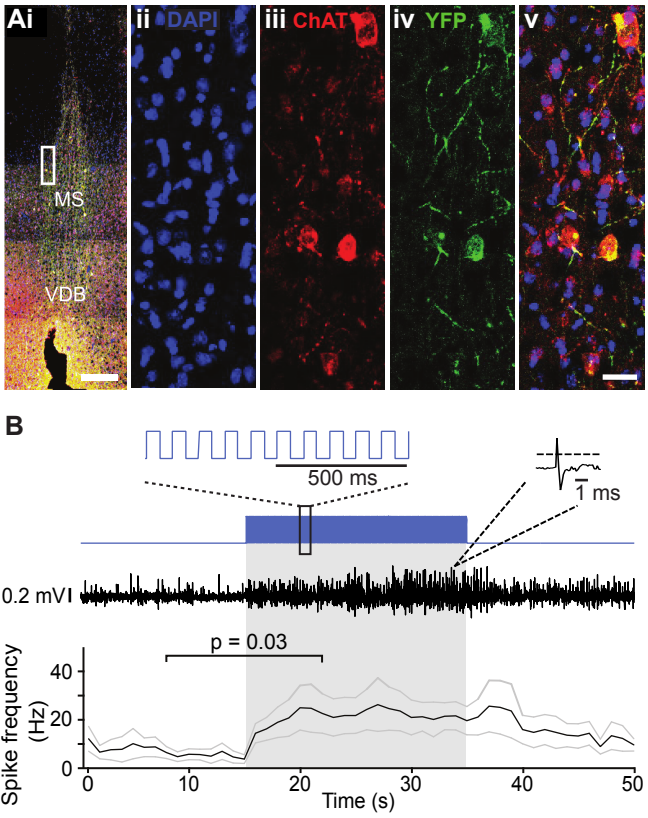
Ai
ii DAPI
iii ChAT
iv YFP
v
MS
VDB
B
500 ms
1 ms
0.2 mV
p = 0.03
Spike frequency (Hz)
40
20
0
0
10
20
30
40
50
Time (s)

Figure 2

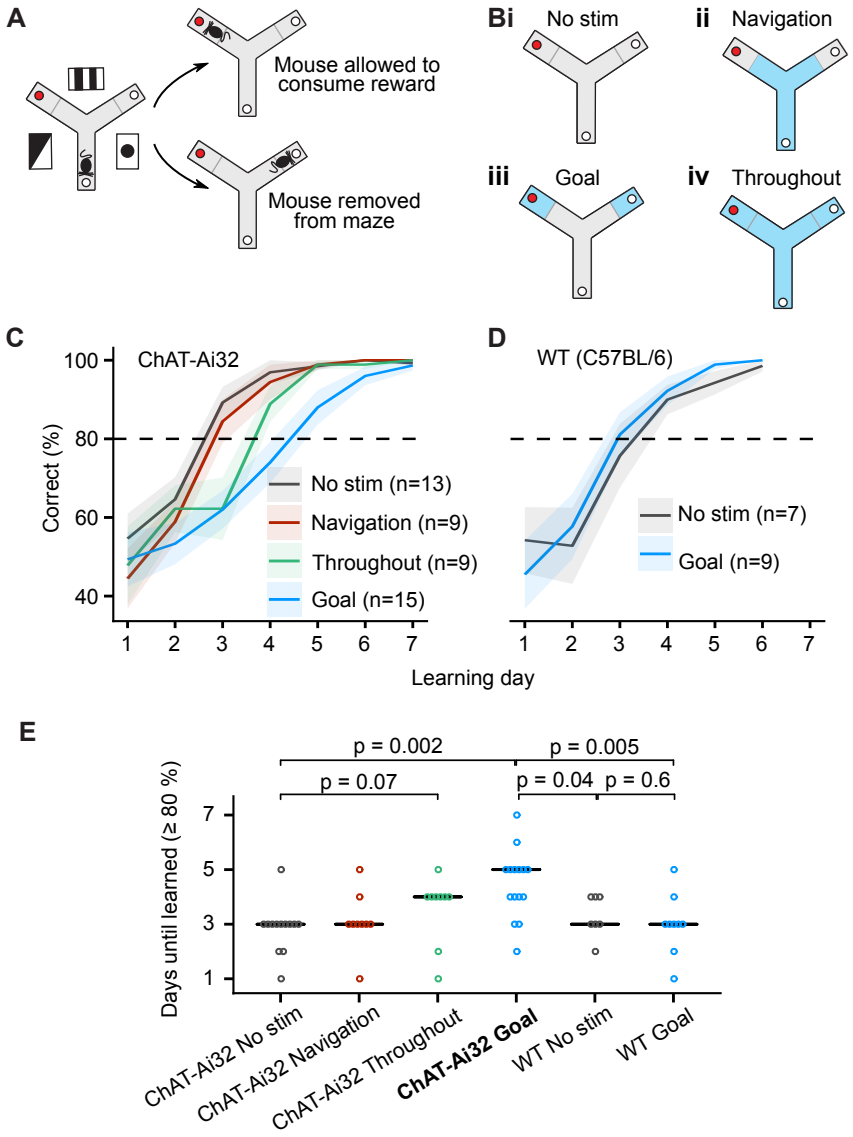
A
Mouse allowed to consume reward
Mouse removed from maze
Bi No stim
ii Navigation
iii Goal
iv Throughout
C
ChAT-Ai32
Correct (%)
100
80
60
40
No stim (n=13)
Navigation (n=9)
Throughout (n=9)
Goal (n=15)
1 2 3 4 5 6 7
D
WT (C57BL/6)
No stim (n=7)
Goal (n=9)
1 2 3 4 5 6 7
Learning day
E
p = 0.002
p = 0.005
p = 0.07
p = 0.04
p = 0.6
Days until learned (≥ 80 %)
7
5
3
1
ChAT-Ai32 No stim
ChAT-Ai32 Navigation
ChAT-Ai32 Throughout
ChAT-Ai32 Goal
WT No stim
WT Goal

Figure 3

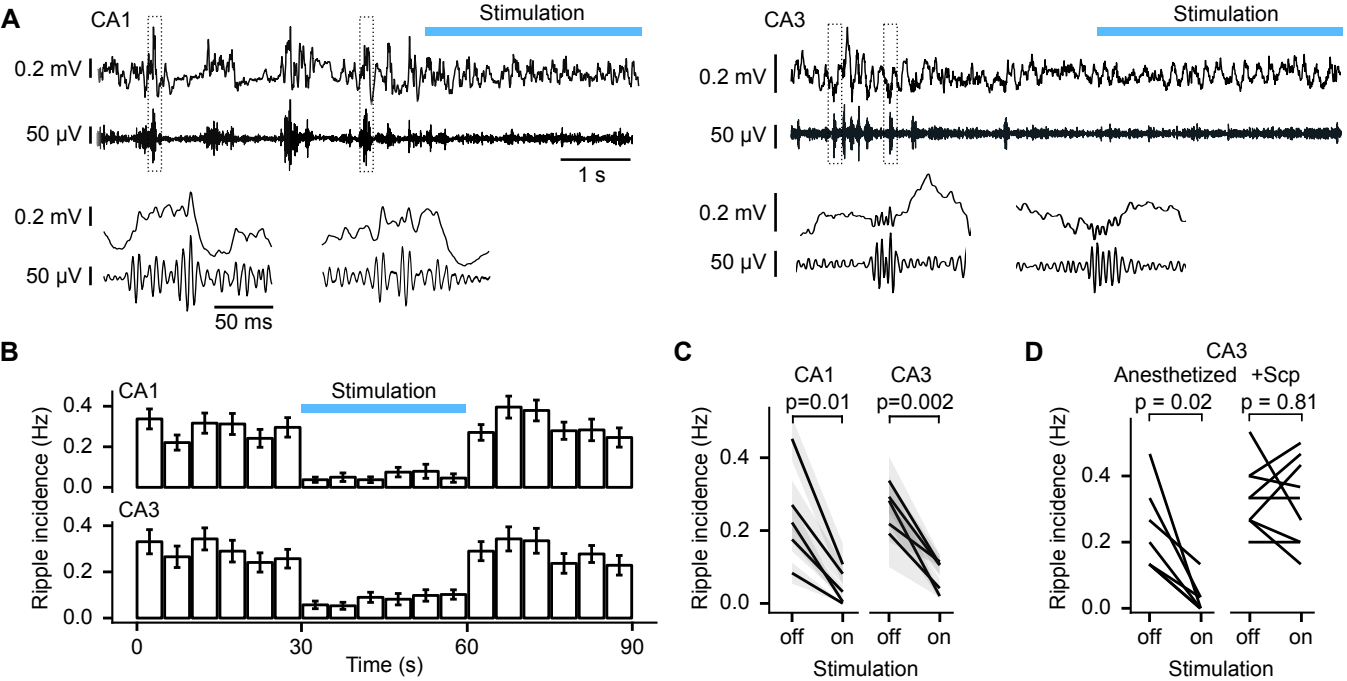
A
CA1
Stimulation
0.2 mV
50 µV
1 s
0.2 mV
50 µV
50 ms
CA3
Stimulation
0.2 mV
50 µV
0.2 mV
50 µV
B
CA1
Stimulation
CA3
Ripple incidence (Hz)
0.4
0.2
0.0
0
30
60
90
Time (s)
C
CA1
CA3
p=0.01
p=0.002
Ripple incidence (Hz)
0.4
0.2
0.0
off
on
off
on
Stimulation
D
CA3
Anesthetized
+Scp
p = 0.02
p = 0.81
Ripple incidence (Hz)
0.4
0.2
0.0
off
on
off
on
Stimulation

Figure 4

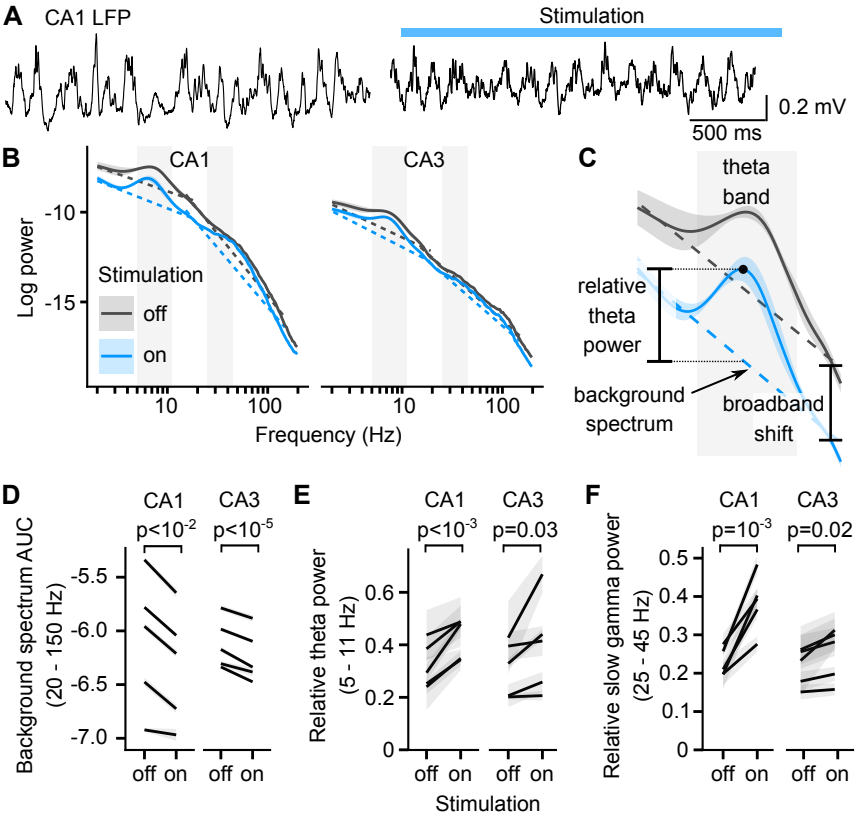
A
CA1 LFP
Stimulation
0.2 mV
500 ms
B
CA1
CA3
Log power
-10
-15
Stimulation
off
on
10
100
Frequency (Hz)
C
theta
band
relative
theta
power
background
spectrum
broadband
shift
D
CA1
CA3
p<10-2
p<10-5
Background spectrum AUC
(20 - 150 Hz)
-5.5
-6.0
-6.5
-7.0
off on
E
CA1
CA3
p<10-3
p=0.03
Relative theta power
(5 - 11 Hz)
0.6
0.4
0.2
0
Stimulation
F
CA1
CA3
p=10-3
p=0.02
Relative slow gamma power
(25 - 45 Hz)
0.5
0.4
0.3
0.2
0.1
0

Figure 5

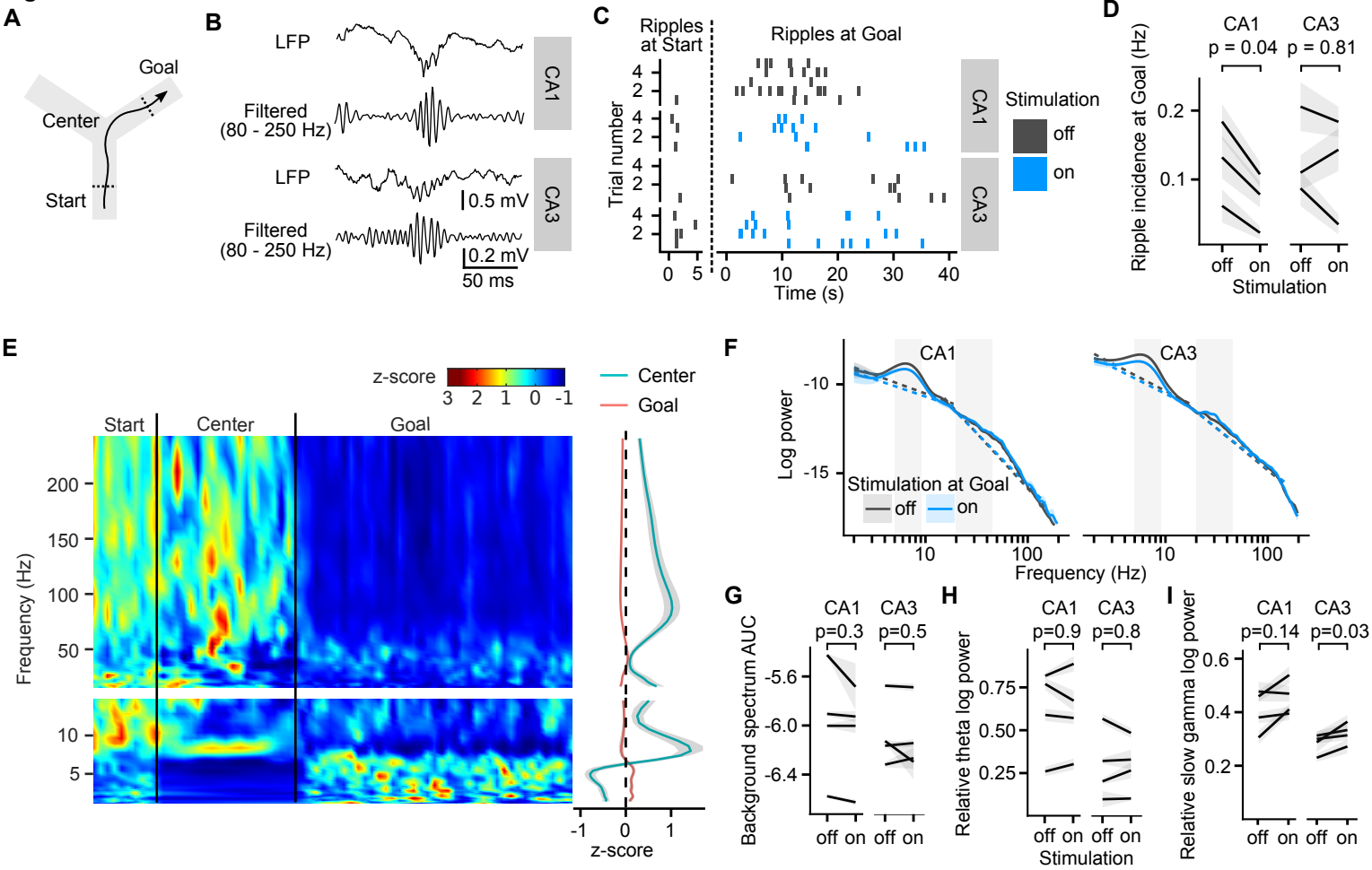
A
Goal
Center
Start
B
LFP
Filtered
(80 - 250 Hz)
CA1
LFP
0.5 mV
Filtered
(80 - 250 Hz)
0.2 mV
50 ms
CA3
C
Ripples
at Start
Ripples at Goal
Trial number
Time (s)
Stimulation
off
on
D
CA1
p = 0.04
CA3
p = 0.81
Ripple incidence at Goal (Hz)
Stimulation
E
z-score
Start
Center
Goal
Frequency (Hz)
Center
Goal
z-score
F
CA1
CA3
Log power
Stimulation at Goal
off
on
Frequency (Hz)
G
CA1
p=0.3
CA3
p=0.5
Background spectrum AUC
H
CA1
p=0.9
CA3
p=0.8
Relative theta log power
Stimulation
I
CA1
p=0.14
CA3
p=0.03
Relative slow gamma log power

Figure 2 - figure supplement 1: Optical fiber implant placement

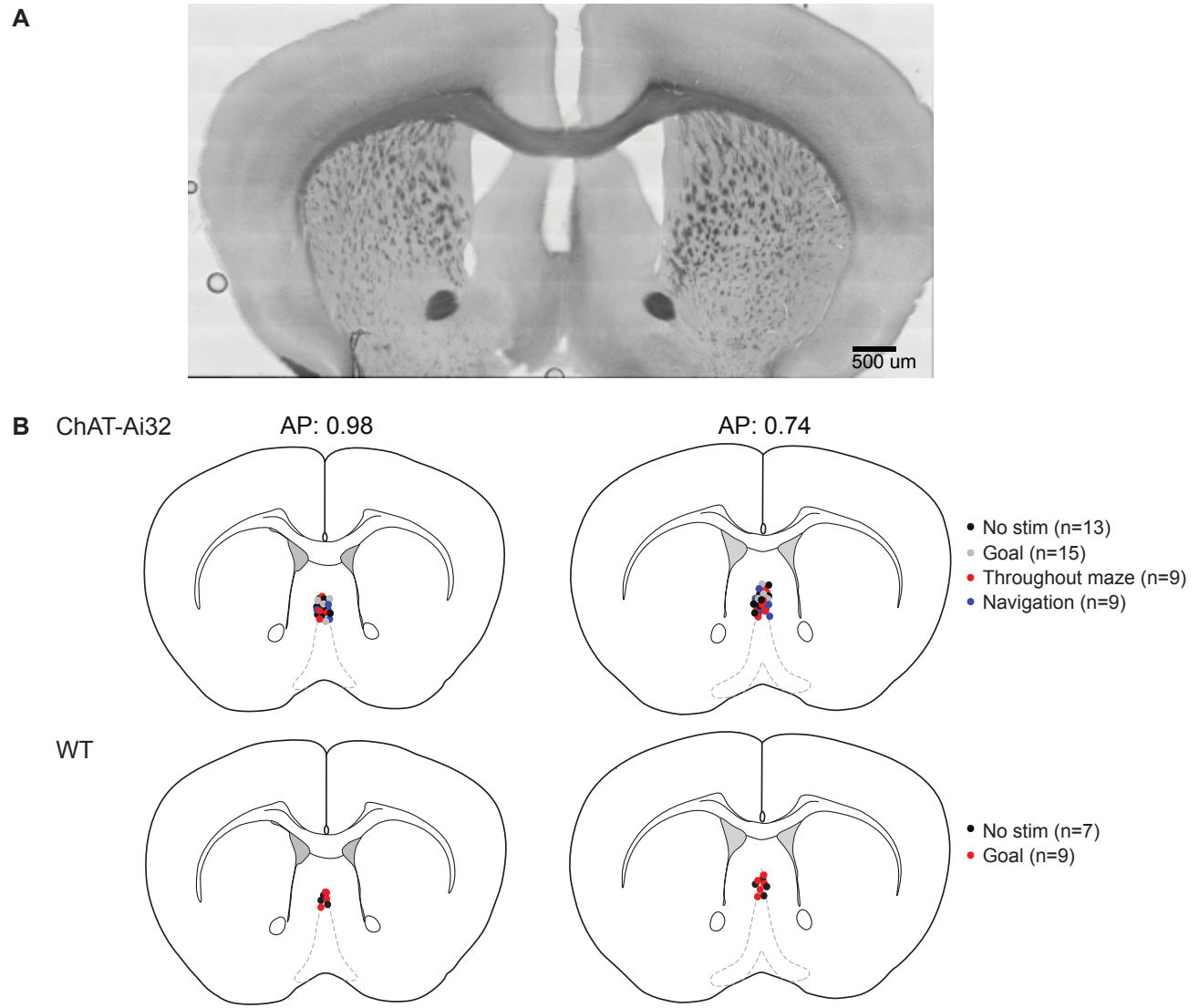

Figure 4 - figure supplement 1: Animal PSD

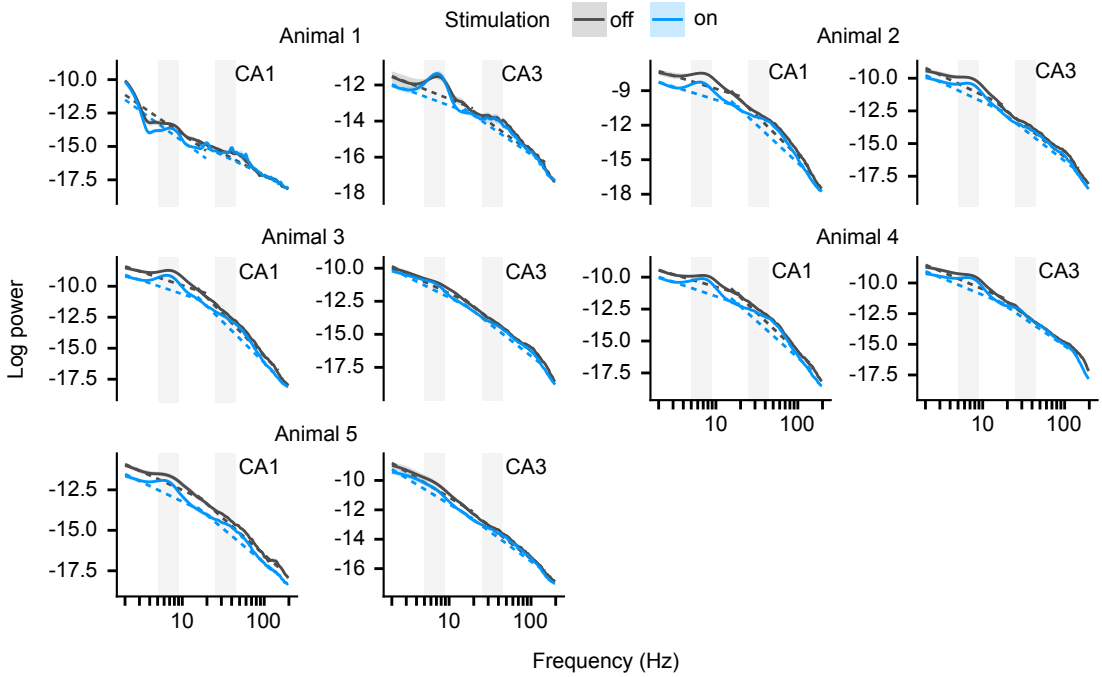
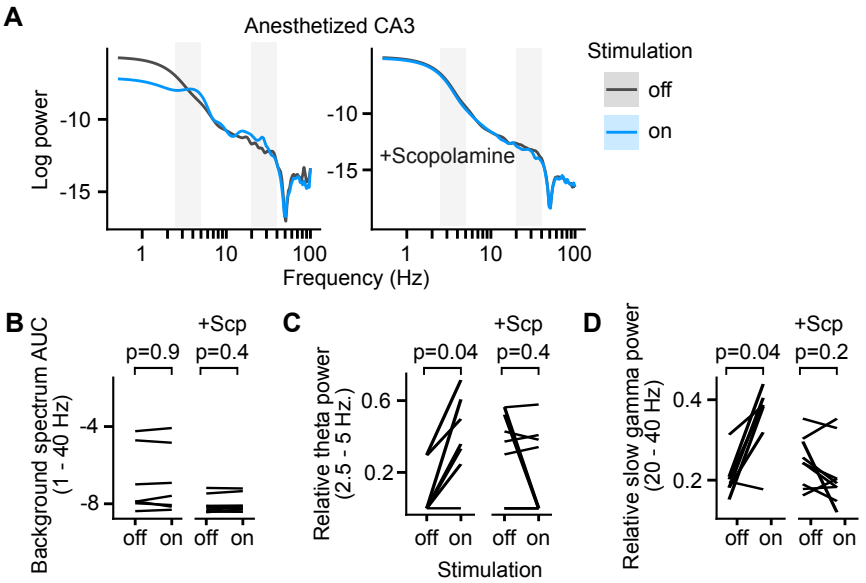
Figure 4 - figure supplement 2: Anesthetized recordings